Geomechanics and Engineering, *Vol. 24, No. 5 (2021) 431-441*
DOI: https://doi.org/10.12989/gae.2021.24.5.431

Centrifuge modelling of rock-socketed drilled shafts under uplift load

Sunji Park[1], Jae-Hyun Kim*[2], Seok-Jung Kim[3], Jae-Hyun Park[3], Ki-Seok Kwak[4] and Dong-Soo Kim[5]

[1]*Centre for Offshore Foundation Systems, The University of Western Australia, 35 Stirling Highway, Crawley, WA 6009, Australia*
[2]*Department of Civil Engineering, Kangwon National University, 1 Kangwondaehak-gil, Chuncheon-si, Gangwon-do 24341, Republic of Korea*
[3]*Department of Infrastructure Safety Research, Korea Institute of Civil Engineering and Building Technology (KICT), 283, Goyang-daero, Ilsanseo-gu, Goyang-si, Gyeonggi-do, 10223, Republic of Korea*
[4]*Underground Space Safety Research Center, Korea Institute of Civil Engineering and Building Technology (KICT), 283, Goyang-daero, Ilsanseo-gu, Goyang-si, Gyeonggi-do, 10223, Republic of Korea*
[5]*Department of Civil and Environmental Engineering, Korea Advanced Institute of Science and Technology (KAIST), 291 Daehak-ro, Yuseong-gu, Daejeon 34141, Republic of Korea*

(Received January 12, 2021, Revised February 10, 2021, Accepted February 16, 2021)

Abstract. Rock-socketed drilled shafts are widely used to transfer the heavy loads from the superstructure especially in mountainous area. Extensive research has been done on the behavior of rock-socketed drilled shafts under compressive load. However, little attention has been paid to uplift behavior of drilled shaft in rock, which govern the overall behavior of the foundation system. In this paper, a series of centrifuge tests have been performed to investigate the uplift response of rock-socketed drilled shafts. The pull-out tests of drilled shafts installed in layered rocks having various strengths were conducted. The load-displacement response, axial load distributions in the shaft and the unit skin friction distribution under pull-out loads were investigated. The effects of the strength of rock socket on the initial stiffness, ultimate capacity and mobilization of friction of the foundation, were also examined. The results indicated that characteristics of rock-socket has a significant influence on the uplift behavior of drilled shaft. Most of the applied uplift load were carried by socketed rock when the drilled shaft was installed in the sand over rock layer, whereas substantial load was carried by both upper and lower rock layers when the drilled shaft was completely socketed into layered rock. The pattern of mobilized shaft friction and point where the maximum unit shaft friction occurred were also found to be affected by the socket condition surrounding the drilled shaft.

Keywords: rock-socketed drilled shaft; uplift behavior; centrifuge modelling; rock

1. Introduction

Rock-socketed drilled shafts have many potential advantages since they efficiently transfer heavy loads from the superstructure by shaft friction between the rock and drilled shaft with smaller displacements. With the advancements in drilling equipment and construction techniques that allow size versatility and installation at almost any ground condition with minimum noise, vibration and disturbance, drilled shafts have become the dominant foundation type for carrying high-foundation loads in various geological settings all around the world (Horvath and Kenny 1979, Rosenberg and Journeaux 1976, Rowe and Armitage 1987, Kulhawy 1991).

In practice, the load applied to a working drilled shaft in rock may include a significant uplift component. Examples include tall and slender structures like transmission tower structures and tall plants that are exposed to overturning moments due to the wind load. Additionally, the foundation for a bridge pier consists of multiple shafts underneath a footing or pile cap, is often subjected uplift load. In the offshore environment, structures whose foundations are in underwater like jetting structure, submerged platforms, and mooring systems, are often loaded upward by buoyancy forces, repeated wind and wave actions (El Naggar and Wei 2000, Goel and Patra 2007, Gaaver 2013, Kim and Rosher 2019). The rock-embedded tension-piles, recognized as the potential foundation solution for providing large uplift resistance to the buoyancy of the submerged floating tunnel (SFT) (Gao *et al.* 2009, Yarramsetty *et al.* 2019), is another example.

The main difference between the compressive load and uplift load is the contribution of the end-bearing component of the end area of the drilled shaft to the total resistance. When a drilled shaft is loaded in uplift, most of the applied loads are resisted by the frictional side resistance developed between shaft and rocks and the self-weight of the drilled shaft (Yang *et al.* 2018, Ashour and Abbas 2020, Pu *et al.* 2020). The end bearing in uplift would equal to the minimum tensile strength of rock or the cohesion between the rock and concrete, multiplied by the tip area. Typically, this value is very low because the normal construction practices potentially lead to a disturbed bottom of a socket hole in the process of crushing the rock. Thus, it is reasonable to disregard tensile resistance developed at the tip under normal uplift circumstances (Kulhawy 2004).

Various field and experimental studies have investigated the empirical correlations between the strength of intact rock and the ultimate unit shaft resistance of the rock-

*Corresponding author, Assistant Professor
E-mail: jaehyun2@kangwon.ac.kr

ISSN: 2005-307X (Print), 2092-6219 (Online)

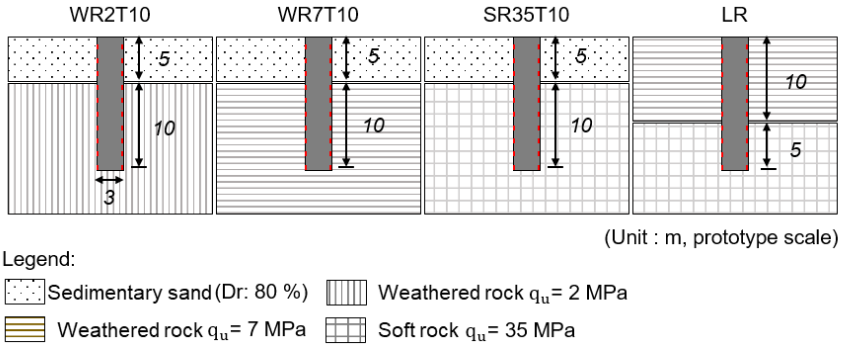

Fig. 1 Test layouts

socketed drilled shaft under compressive loading, such as Horvath and Kenny (1979), Rowe and Amitage (1987), Reese and O'Neill (1988), and Kulhawy and Carter (1988). In current design practice, uplift resistance is estimated with these empirical design methods, considering reduction factors in shaft resistance since piles have lower uplift capacity than their compression shaft resistance (AASHTO 2007, FHWA 2010). However, it is generally understood that the unit friction for compressive loading and tensile loading is different since compressive loading tends to increase the stress acting on the rock and thereby increase the rock strength, whereas the tensile loading has the opposite effect (Chang *et al.* 2006). Nevertheless, little has been investigated on the uplift behavior of rock-socketed drilled shaft in the model test under appropriate stress conditions that can quantitatively evaluate the skin friction behavior between the rock and drilled shaft.

In this study, a series of centrifuge tests have been performed to investigate the uplift response of rock-socketed drilled shafts. In a geotechnical centrifuge, the rock-foundation interface interaction, is well simulated because the magnitude of confining stresses of a prototype drilled shaft and the lateral stiffness of the surrounding rock is realistically created in an enhanced gravity field (Leung and Ko 1993, Dykeman and Valsangkar 1996, Xing *et al.* 2014). In addition, axial loads up to several hundred mega-newton (MN) that required to bring the prototype rock-socketed drilled shaft to failure can be simulated effectively with a smaller model load in a centrifuge according to the established scaling relationship [i.e., $F_{model} = F_{prototype}/N^2$, here, F_{model} and $F_{prototype}$ indicate the force in model scale and prototype scale, respectively, and N means the centrifugal acceleration ratio compared to the Earth gravity (g)]. Also, together with uniform and measurable geotechnical material properties and quantitative measurements, the full-scale performance of drilled shaft can be effectively simulated and investigated in a relatively controllable environment.

In the paper, the uplift load-displacement responses of the drilled shafts installed in various rock sockets are presented through the interpretation of the test results of geotechnical centrifuge test. The strain gage measurements are used to investigate the load distribution in the shaft during the uplift loading. The results are also used to observe the distribution and allocation of mobilized side friction between the rock and shaft under the working loads to failure conditions.

2. Centrifuge modelling

2.1 Modelling of rocks

In this study, the drilled shafts were socketed in different rock conditions as illustrated in Fig. 1 and tabulated in Table 1. WR2T10 and WR7T10 simulated drilled shafts partially socketed into weathered rock having unconfined compressive strength (q_u) of 2 MPa and 7 MPa with 10 m of thickness, respectively. Similarly, SR35T10 simulated a drilled shaft partially socketed into soft rock having q_u = 35 MPa with 10 m of thickness. LR simulated a completely socketed drilled shaft in a layered rock consists of overlying

Table 1 Model test program and ground conditions (in prototype scale)

Test ID	Sand		Rocks			
			WR		SR	
	t (m)	D_r (%)	t (m)	q_u (MPa)	t (m)	q_u (MPa)
WR2T10	5	80	10	2	-	-
WR7T10	5	80	10	7	-	-
SR35T10	5	80	-	-	10	35
LR	-	-	10	7	5	35

*WR: weathered rock, SR: soft rock, t: layer thickness, D_r: sand relative density, q_u: unconfined compressive strength (UCS)

Table 2 Characteristics of mixes for artificial model rocks

Rock type		WR2	WR7	SR35
Unit weight (t/m^3)		1.42	1.52	2.32
q_u (MPa)	Curing time 3-days	2.06	6.36	32.4
	Curing time 5-days	2.33	6.67	33.6
v_L (m/s)		1,203	2,227	3,776
v_s (m/s)		717	1357	2381
ν		0.41	0.34	0.26
E (GPa)		2.05	8.74	32.58

*WR2: weathered rock of 2 MPa, WR7: weathered rock of 7 MPa, SR35: soft rock of 35 MPa, q_u: unconfined compressive strength, v_L: longitudinal propagation velocity, v_s: shear wave velocity, ν: Poisson's ratio, E: Young's modulus

Table 3 Properties of silica sand

Items	Properties
Specific gravity, G_s	2.65
Fin contents passing #200 (%)	0.9
Max. dry density* (t/m^3)	1.58
Min. dry density** (t/m^3)	1.26
Grain size (mm)†	D_{10} = 0.19
	D_{50} = 0.32
	D_{60} = 0.34
Soil classification‡, USCS	SP
Uniformity coefficient, C_u	1.71
Coefficient of curvature, C_c	1.16

*ASTM D 1557-07 (ASTM 2007)

**ASTM D4254-00 (ASTM 2006)

†D_{10}, D_{50}, D_{60}: effective particle size corresponding to 10%, 50%, and 60% finer on particle size curve

‡ ASTM D 2487-11 (ASTM 2011)

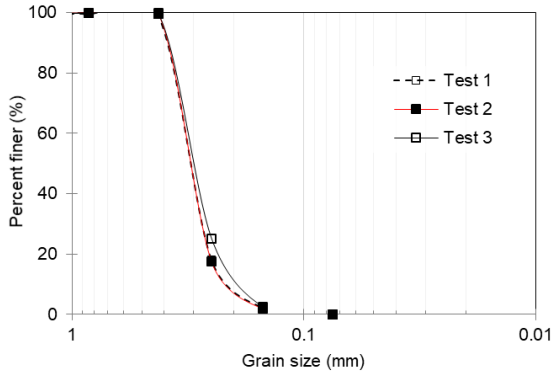

Fig. 2 Grain size distribution for silica sand

Table 4 Dimensions of drilled shaft model

	Model	Prototype (at 50 g)
Diameter	0.060 m (external)	3 m (external)
	0.048 m (internal)	
Length	0.30 m	15 m
Material	Aluminium alloy *(Al 6061)*	Concrete drilled shaft
Young's modulus	69 GPa	23.5 GPa
Weight	9.8 N	1.23 MN

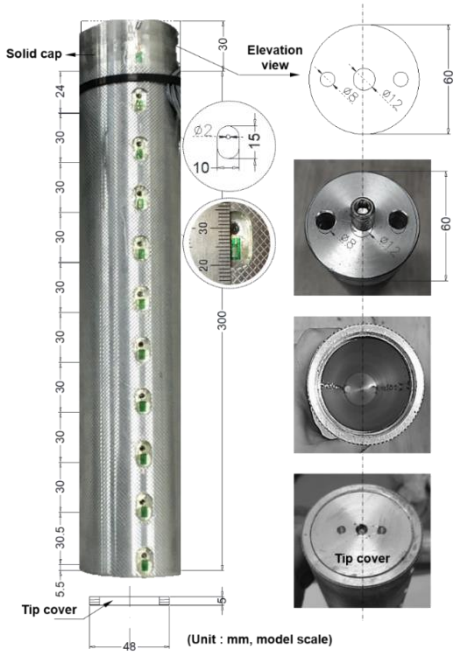

Fig. 3 Model drilled shaft used in this study

weathered rock of q_u = 7 MPa and underlying soft rock of q_u = 35 MPa. The target q_u of the specimen was determined according to the rock classification based on the elastic wave velocity in the Korean standard (KICT 2017).

A cement-sand mixture and a dry mortar were used to simulate the weathered rock and soft rock, respectively. A preliminary study was conducted in order to investigate and determine the mix proportions for the desired artificial model rock with the target compressive strength. Artificial crushed silica sand, mortar, and water were mixed in various ratios to make a 50 mm square standard specimen (KICT 2017). Throughout numerous trials, it was found that sand:cement:water = 1:0.07:0.035 and 1:0.15:0.075 (for q_u = 2 and 7 MPa, respectively) with 0.5 water-cement ratio, and dry mortar:water ratio by mass of 1:0.1 (for q_u = 35 MPa) can reproduce the desired model rock uniaxial strength. Also, the preliminary tests using the 50 mm square specimens showed that the compressive strength of artificial rock stabilized after three curing days at room temperature. Subsequently, all the centrifuge tests were performed exactly same days after the sample preparation. In addition, additional unconfined compressive tests using the 50 mm square specimens prepared by the particular batch of cement mix were performed on the same day of the centrifuge tests.

Free-free resonant column (FFRC) tests were also conducted to evaluate the strength and stiffness characteristics of the specimen. The properties of artificial model rocks are tabulated in Table 2. The results show that the obtained values were very similar to the properties for real weathered rock and soft rock, considering that compressive strength rages of actual weathered and soft rock distributed in Korea are 2-7 MPa and 35 MPa, respectively.

For sand layer, dry silica sand was used. Table 3 and Fig. 2 describe the key physical properties of the silica sand. The detailed properties of silica sand can be found in Kim *et al.* (2016).

2.2 Modelling of drilled shafts

A drilled shaft model with dimensions as in Table 4 was used in this study. The dimensions are chosen such that their sizes are frequently used in the field. An aluminium alloy was used to simulate the prototype drilled shaft with a diameter of 3 m and a length of 15 m, which is a typical diameter and the maximum depth (length) possible to construct in the site for the electric transmission tower. The

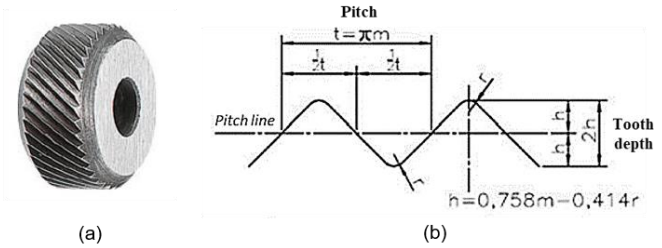

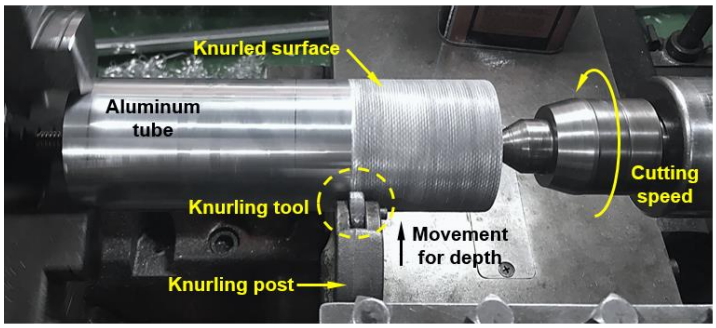

Fig. 4 Knurling method for simulating socket wall roughness; (a) knurling tool (Module #18), (b) tooth depth definition and calculation and (c) photograph showing knurling operations on the aluminium tube surface

similarity between the model and the prototype in terms of an equivalent axial stiffness (EA) was calculated as follows:

$$E_m \frac{\pi}{4}\left(D_m^2 - d_m^2\right) = \frac{1}{N^2} E_p \frac{\pi}{4}\left(D_p^2\right) \quad (1)$$

where E is Young's modulus, D and d are the outer and inner diameters, N is the similarity ratio which is 50 in this study, and the prototype and model drilled shafts are represented by subscript 'm' and 'p', respectively. By assuming that the Young's modulus of concrete and aluminum is 23.5 GPa (E_p) and 69 GPa (E_m), respectively, the outer and inner diameters of the aluminium model tube were selected as D_m = 60 mm and d_m = 48 mm to match the Young's modulus of the drilled shaft made of concrete (see Fig. 3).

The roughness of the drilled shaft was modelled by knurling of the surface of the aluminium tube. Knurling enabled selected value of roughness height can be quite correctly implemented with a specified knurling tool (see Fig. 4(a)). The roughness height of 7.5 mm in prototype scale was employed as suggested by Lee *et al.* (2003), which is suggested roughness height of the socket wall considering the uniaxial compressive strength of the intact rock. It should be mentioned that the roughness height of 2.6 mm, which is smaller than the value applied in the model, would better simulate the socket wall for the soft rock of 35 MPa. However, the value of 7.5 mm was adopted here to avoid the scale effect on the mobilized shear stress on the rock-drilled shaft interface under the high centrifugal acceleration as reported by Kishida and Uesugi (1987).

The model drilled shaft was instrumented with 10 pairs of strain gage affixed symmetrically at 10 levels (a spacing of 30 mm in model scale) to evaluate the load transfer between the drilled shaft and the rock.

3. Experimental program

3.1 Centrifuge facility

The experimental program was carried out in the geotechnical centrifuge at the Korea Advanced Institute of Science and Technology (KAIST). All the tests described in this paper were carried out at accelerations of 50g. More details and specifications of the centrifuge are given by Kim (2013).

3.2 Model preparation

The models for all the centrifuge tests were prepared in a cylindrical rigid steel container having an internal dimension of 900 mm (diameter) × 700 mm (height). Additionally, a cylindrical model casting mold with a dimension of 845 mm (diameter) × 450 mm (height) was created for rock model preparation. The mold has a slightly smaller size of the model container so that it can be placed inside the model container after curing the artificial rock. The gap between the container and the mold filled with sand to prevent deformation or movement of the mold during the test.

The silica sand and cement were mixed by using an electric concrete mixer prior to the addition of water and retarder in order to prevent lumps. Subsequently, tap water at room temperature with the dissolved retarder was added to the dry cement-sand constituent and thoroughly mixed. The blended mixture was poured into the casting mold and compacted into five layers to form a sub layer that model drilled shaft can be placed. After levelling the surface of the sub layer, the model drilled shaft was placed by using a guide developed for positioning model drilled shaft in a proper location to make an accurate connection with the

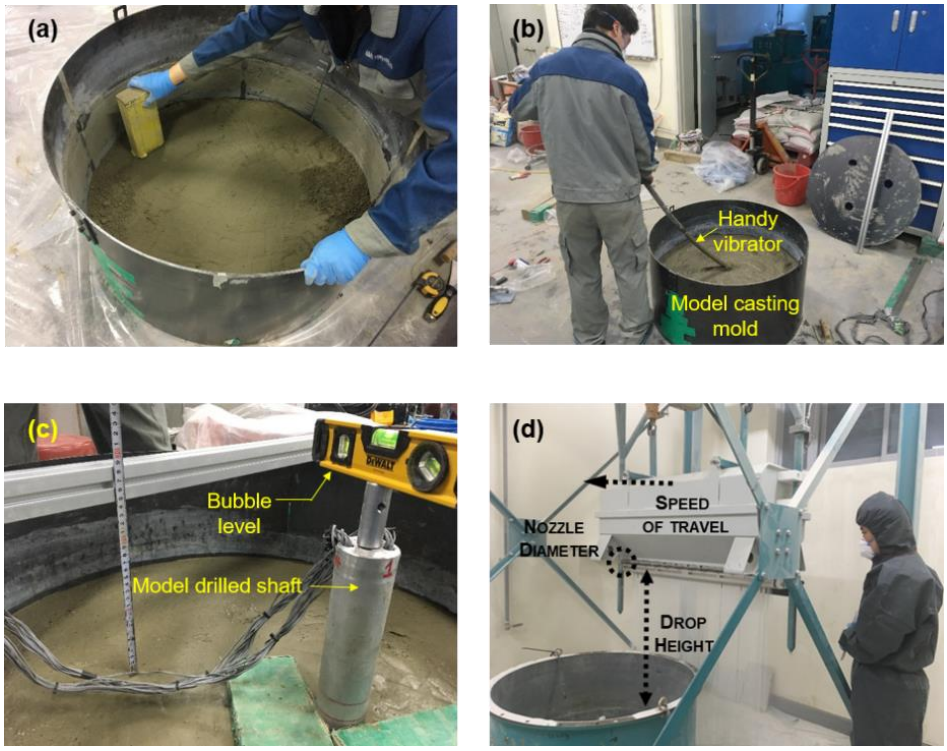

Fig. 5 Photographic series depicting model preparation procedures; (a) weathered rock layer compaction, (b) construction of soft rock layer by concrete vibrator, (c) positioning and levelling of drilled shaft and (d) sand pluviation using an automatic sand hopper

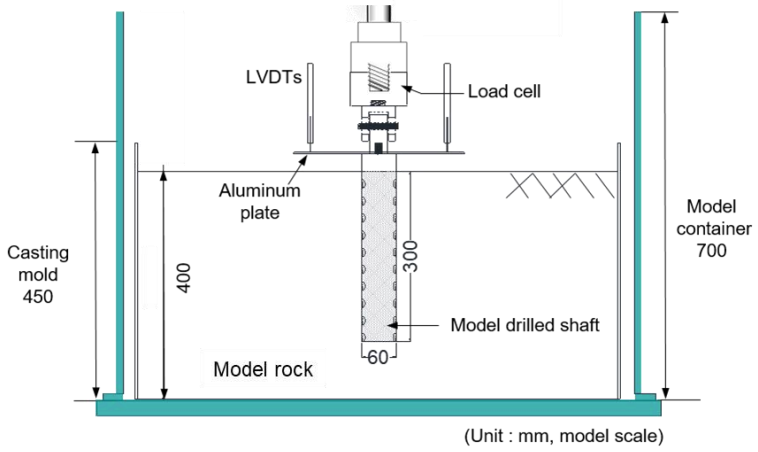

Fig. 6 Test set-up

loading system. The prepared cement-sand mortar was then poured, and areas surrounding the shaft were compacted into additional layers to fix the model drilled shaft. Between compaction of each layer, proper chipping with sharp pointer was employed to ensure the connection of layers. Both horizontal and vertical levelness of the model drilled shaft were also checked using a digital level meter throughout the model preparation. The model was then allowed to harden at room temperature for three to five days to achieve the desired compressive strength.

Soft rock preparation has a similar process as that of weathered rock. By using the large pan mixer, the Remitar mixture was homogeneously combined and poured into the mold. A handy concrete vibrator was used to settle the mortar mixture. When a model drilled shaft was placed in a proper location of the sub layer, another prepared Remitar mixture filled the surrounding areas of drilled shaft giving desired embedment depth. Also, a poking with a steel rod was necessary to eliminate the trapped air. The model was then cured at room temperature for three to five days.

For a model construction for layered rock, the smooth surface of the soft rock model was harshly roughened by using a hand abrasive grinder thus creating more frictional surface areas which weathered rock material can adhere. Extra care must be taken to make ensure that the two layers are not separated during the loading test. After the roughened surface obtained, weathered rock mixture was placed and compacted in a similar procedure mentioned

above. This ensured the bond between two different model rocks.

The overlying sand layer was created using an automated sand hopper. Once the appropriate embedment depth was achieved the surface of pluviated sand was levelled. Finally, the relative density of the sand was measured.

3.3 Centrifuge test procedures and instrumentations

A typical test set up is presented in Fig. 6. The load cell was equipped between the head of the drilled shaft and actuator to measure the applied uplift load. Two LVDTs (Linear Variable Differential Transformer) were fixed vertically on an aluminium plate slotted onto the pile head to measure the vertical displacement of the drilled shaft under loading. An additional LVDT was placed at a boundary of the container and the movements of the model container and mold were also carefully monitored. Ten pairs of strain gages were attached to external surface of drilled shafts and measured the strain values during the load test.

After the sensors and devices arrangement, signals from the sensors were monitored through the data acquisition system and control of loading systems were checked to insure they were working. When everything was in place and working properly the centrifuge started. The centrifugal acceleration was gradually increased to 50 g at a rate of 2 g/min and stabilized at 50 g for about five minutes. This acceleration was maintained during the load test.

The load tests for tests WR2T10 and WR7T10 were performed by a vertical actuator (maximum capacity of -20 kN) and tests SR35T10 and LR were performed by a hydraulic jack (maximum capacity of -50 kN). The actuators were tightly connected to the rigid frame fixed on top of the container. Tests were carried out by displacement control at 0.01 mm/s and this corresponds to a procedure E: Constant rate of uplift in ASTM D3689-07. All the tests were terminated after observing a failure (determination of failure is discussed in Section 4.1).

4. Test results and analysis

In total, four model drilled shafts socketed in the different rocks were tested as schematically represented in Fig. 1. These testing schemes were designed to evaluate the uplift load-displacement and uplift capacity of the rock-socketed drilled shaft with respect to rock compressive strength and also to investigate the load transfer and skin friction mobilization characteristics depending on the types of rock sockets. All the results presented in this paper been scaled to represent the prototype.

4.1 Load-displacement response

Fig. 7 shows load-displacement curves for four drilled shafts in different rock conditions. Uplift load was measured by the load cell connected between the end of the actuator and the top of the model drilled shaft, and upward movement was measured at the top of the model drilled shaft. It clearly shows two distinct shapes of load-

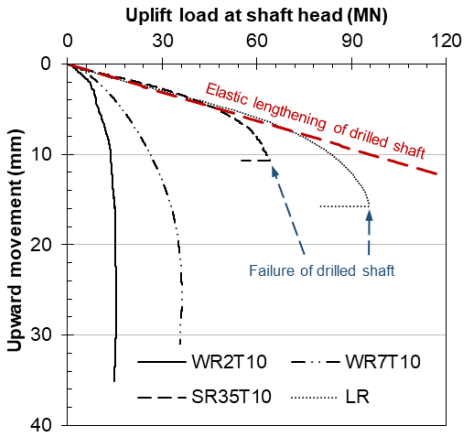

Fig. 7 Load-displacement response of rock-socketed drilled shaft under uplift load

Table 5 Ultimate load criteria for axial uplift load tests (modified from Hirany and Kulhawy 1988)

Basis of definition	Interpreted failure load definition	Author/Agency/ Code/Reference
Displacement rate limitation (function of load)	Load at which plastic curve breaks sharply	Chellis (1961)
	Load at which total settlement increases without a further load increase	Tomlinson (1977)
Absolute displacement limitation	Load at total displacement of 12.7 mm (0.5 in.)	Hirany and Kulhawy (1988)
	Load at total displacement of 6.25 mm (0.25 in.)	Parkash and Sharma (1990)
Relative displacement limitation	Load that gives a displacement equal to the elastic elongation of pile plus 4 mm (0.15 in.)	Fuller (1983)

displacement curves depending on the strength of the rock sockets. For the drilled shafts in SR35T10 and LR where the rock socket is stronger and stiffer, had a linear response to the failure load. This linear relationship was nearly identical to the elastic elongation line of the model drilled shaft, PL/AE, in which P = uplift load, L = length of the drilled shaft, A = area, and E = Young's modulus. This indicates that rock-socketed drilled shaft under uplift load shall behave as rigid when socketed in highly stiff layers which also follows the field test results (Carter and Kulhawy 1992).

On the other hand, the load-displacement curves for WR2T10 and WR7T10 exhibit three different regions: an initial linear hardening region with high stiffness; a transition zone from linear to nonlinear response with an increase in the applied load; and finally, a "plunging point" where the load-displacement curve is nearly horizontal (i.e., slope ≈ 0) as described in Livneh and El Naggar (2008). After the plunging point, the displacement of the model drilled shaft WR2T10 and WR7T10 increased sharply and disproportionately to more than 30 mm until the test terminated.

From the load-displacement curve, the ultimate capacity (Q_u) was obtained for each test. Several methods were available in the literature as summarized in Table 5. Although these interpretation methods are originally proposed for the compression test, the general shapes of the load-displacement curves for compression and uplift tests

Table 6 Net ultimate uplift load capacities and their corresponding displacement of drilled shaft

Test ID	Q_n^* (MN)	u_n^* (mm)
WR2T10**	11.67	6.81
WR7T10**	31.67	14.57
SR35T10‡	62.88	9.78
LR‡	94.25	14.24

*Q_n: net ultimate load capacity of a drilled shaft (= Q_u -W_d), u_n: upward movement corresponding to the net ultimate load capacity of a drilled shaft

**ultimate capacity (Q_u) determined by Tomlinson (1977) and Parkash and Sharma (1990)

‡ultimate capacity (Q_u) determined by Chellis (1961)

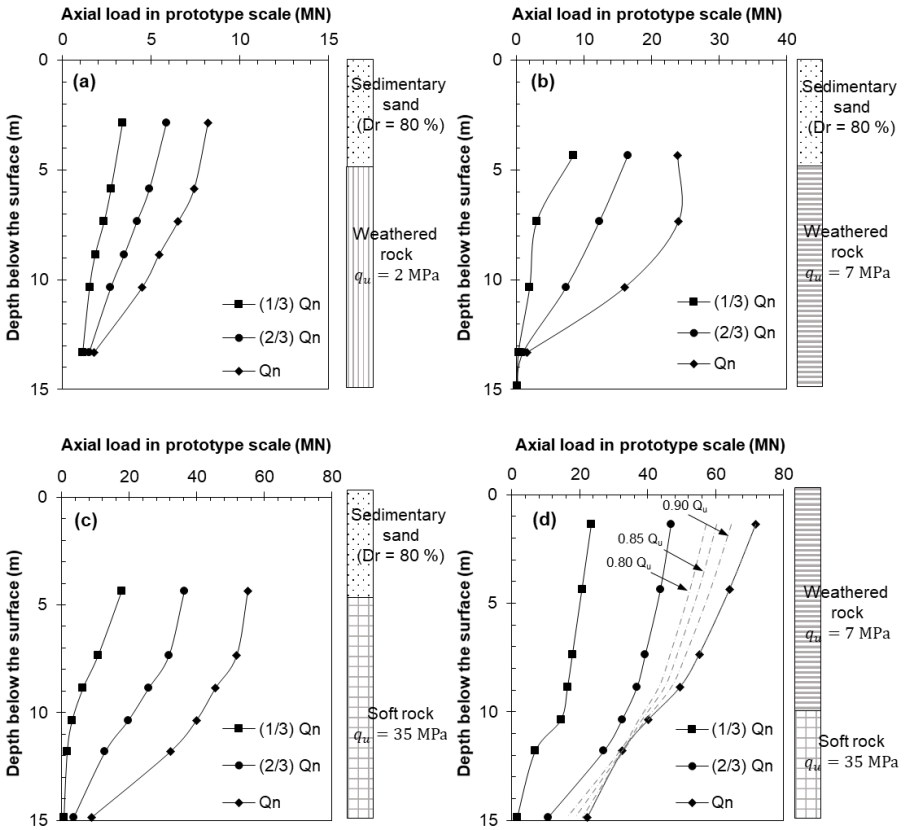

Fig. 8 Load distribution along the drilled shaft at different load increments for (a) WR2T10, (b) WR7T10, (c) SR35T10 and (d) LR

on drilled shafts are similar. Therefore, most of the methods can be applied to define the ultimate load in uplift tests (Hirany and Kulhawy 1988).

For the load-displacement curves of SR35T10 and LR, they had a sharp breakage point, where the uplift load suddenly decreases with large displacement, was considered as the ultimate uplift capacity as described in Chellis's method (1961). For the tests of WR2T10 and WR7T10, the load-displacement curve exhibited a clear plunging failure point. In this case, the ultimate capacity was considered at the point where the displacement is increasing without an increase in the load as suggested by Tomlinson (1977) and Parkash and Sharma (1990). From the determined ultimate uplift capacity, net ultimate uplift capacity (Q_n) was calculated by subtracting self-weight of the drilled shaft (W_d = 9.8 N (in model scale) and 1.23 MN (in prototype scale)). The determined net ultimate uplift capacity and the corresponding displacement for each drilled shaft are summarized in Table 6.

It is generally accepted that the displacements of pile foundations should be limited below normalized displacement of Z/D = 10%, where Z is the measured upward displacement and D is the diameter of model drilled shaft, (both are in prototype scale). For some foundation designs where the principle force is uplift, for example, a foundation for transmission tower, guidelines suggest absolute values of displacement regardless of foundation size, since once the ultimate design load is exceeded, it is hard to stop the foundation displacement. IEEE (2001) suggested that the 13 mm displacement of the pile from the original position was defined as foundation failure. National Grid (2004) suggests the displacement defining failure of 10

Table 7 Load carrying proportion by layers

Test ID	Applied net uplift Load (MN)		Overlying layer		Underlying layer	
			Carried load (MN)	Shared ratio (%)	Carried load (MN)	Shared load ratio (%)
WR2T10	1/3 Q_n	3.89	0.98	25.10	2.91	74.90
	2/3 Q_n	7.78	2.59	33.27	5.19	66.73
	Q_n	11.67	4.03	34.49	7.65	65.51
WR7T10	1/3 Q_n	10.56	3.22	30.45	7.34	69.55
	2/3 Q_n	21.12	5.45	25.82	15.66	74.18
	Q_n	31.67	7.22	24.36	23.96	75.64
SR35T10	1/3 Q_n	20.96	8.27	39.46	12.69	60.54
	2/3 Q_n	41.92	12.36	29.49	29.56	70.51
	Q_n	62.88	15.55	24.72	47.34	75.28
LR	1/3 Q_n	31.42	16.43	52.29	14.99	47.71
	2/3 Q_n	62.84	29.33	46.67	33.51	53.33
	Q_n	94.25	51.80	54.96	42.46	45.04

Note: Q_n is the net ultimate uplift load capacity determined in the Table 6

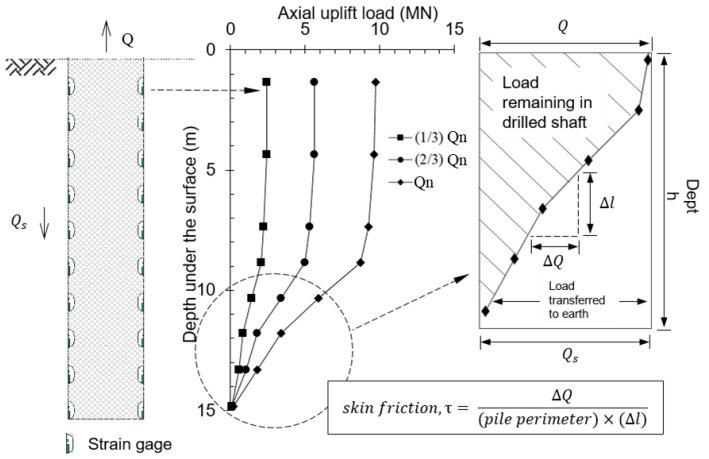

Fig. 9 Instrumentation for determining load in the drilled shaft and skin friction

mm and 7 mm for sand and clay, respectively. Considering 10 mm limit of displacement for mobilizing ultimate capacity, WR2T10 mobilized 14 MN whereas, SR35T10 mobilized 64 MN of uplift load for the same socket depth. This shows that the strength of rock socket significantly influences to uplift load capacity.

4.2 Axial load in the drilled shaft

Based on the strain measured from the strain gauges attached on the external shaft of the drilled shaft, the load transmitted at a particular depth was calculated by the following equation:

$$Q = EA\varepsilon \quad (2)$$

in which Q = load in the drilled shaft at strain gage level, ε = strain measured by the strain gage, A = cross-sectional area of the drilled shaft, and E = Young's modulus of drilled shaft. To eliminate the effects of the bending stress in the shaft, two separate strain gages installed symmetrically for the center of the drilled shaft at the same elevation were averaged.

Fig. 8 shows the axial load distribution profiles along the surface of the drilled shaft. Each curve represents a measurement at one third, two thirds, and the ultimate load (Q_n), where Q_n is the net ultimate uplift load capacity determined in the section 4.1. Unfortunately, due to malfunction of the strain gages, the measurements near the tip in Fig. 8(a) were excluded.

The axial load decreased slightly in the overlying sand layer and decreased steeply when the drilled shaft entered the underlying rock layer. The trend was similar under different levels of applied uplift load. For the test WR2T10, WR7T10, and SRT10 which have 5 m of sand layer over the 10 m of rock, more load was transferred to a stronger and stiffer rock layer. Particularly for WR2T10 (Fig. 8(a)), under each applied-load levels, rock layer carried the 70 ~ 80% of the applied load. Similarly, for WR7T10 (Fig. 8(b)) and SR35T10 (Fig. 8(c)), rock layer shared 82 ~ 94% of the applied load. It can be observed that as the strength of rock-socket increases, the proportion of uplift load carried by the

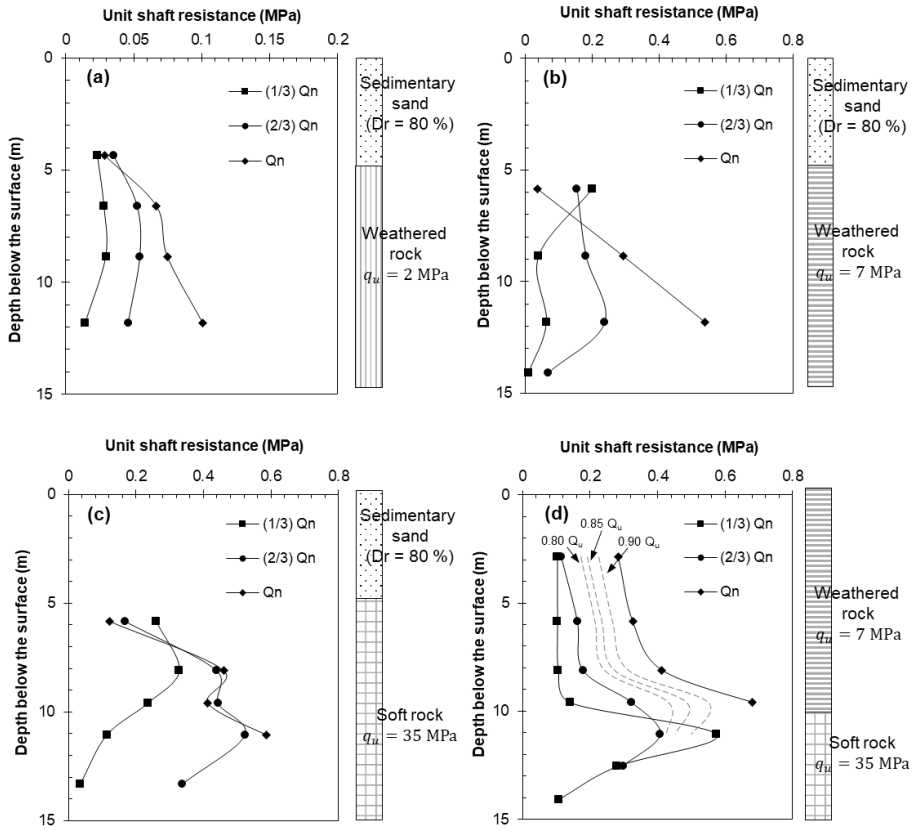

Fig. 10 Shaft resistance distribution of drilled shaft for (a) WR2T10, (b) WR7T10, (c) SR35T10 and (d) LR

rock layer increased.

For the drilled shaft completely socketed in layered rock (Fig. 8(d)), the distribution curve had two different trends of slopes. When the uplift load of 2/3 Q_n or less is applied, almost 50% of the applied load was resisted by stiffer and stronger underlying (soft rock) layer showing a steeper decrease of load at 10~15 m. However, as the uplift load approached to the net ultimate load (Q_n), the load was transferred more to the overlying weathered rock layer (depth of 0~10 m below the surface) and showed a steeper decrease of the load than the underlying layer. Additional grey dotted lines were included in Fig. 8(d) to show the load transfer near the failure condition. It clearly shows that the load transfer becomes more substantial in the overlying layer of weathered rock.

Based on the axial load distribution, the amount of load carried at each layer was calculated. As the strain gage was not located exactly at the boundary of the two layers, the strain readings from the closest sensors above and below the layer boundary were linearly interpolated. Then, the carried load was considered as the total load carried by each layer. In addition, the shared load ratio for each layer was calculated by dividing the carried load at each layer by the applied net uplift load. The results of the carried load and shared load ratio at each load levels (1/3 Q_n, 2/3 Q_n, and Q_n) are tabulated in Table 7.

It should be mentioned that the shafts in soft rocks (SR35T10 and LR) showed some load transfer near the tip. The main reason is that the strain gage attached near the tip was located 5.5 mm above the tip (27.5 cm in prototype scale), therefore the presence of the load transfer from tip to 2.75 cm above the tip was reflected. The strong chemical bonding between the tip cover and the model soft rock material (Remitar) is also suspected to affect the mobilization of resistance near the tip. Thus, the results described in this paper limited to the specific testing conditions.

4.3 Mobilized skin friction along the drilled shaft

Based on the axial load, the unit skin friction was obtained as it is illustrated in Fig. 9. The difference between the axial forces calculated from any two sets of strain gages along the drilled shaft wall represented the total load transferred to the surrounding rock or sand between two points. Then dividing this difference by the corresponding surface area, the average of unit skin friction can be calculated. Again, the strain gage measurements for test WR2T10 were excluded due to the malfunction of the sensor.

Fig. 10 shows the distribution curves of unit skin friction along the shaft. The unit skin friction curves are shown with several load levels correspond to 1/3 Q_n, 2/3 Q_n, and Q_n from the initial load level to failure load. Additional grey dotted lines were included in Fig. 10(d) to show the load transfer near the failure condition.

The graph shows that the skin friction in the underlying layer increased with depth and reached its maximum at a mid-depth the underlying layer (except Fig. 10(a) where strain gage malfunctioned). For example, in Fig. 10(b), the maximum skin friction was mobilized about 12 m below the surface (which is a depth of 2/5 of the thickness of the

underlying layer). For Fig. 10(c), the maximum skin friction was occurred about 8 m below the surface (which is a depth of 4/5 of the thickness of the underlying layer) and Fig. 10(d) showed high skin friction at 12 m below the surface initially and then the maximum skin friction was mobilized at 10 m below the surface which is near the layer boundary.

Then the skin friction decreased at the bottom of the shaft. Fig. 10(a), 10(b), and 10(c) show that the shaft friction was increased greatly in the underlying layer than the sand layer. The mobilized maximum friction was increased with increasing strength of the rock-socket. Fig. 10(d) shows that firstly the skin friction increases greatly in the soft rock layer (at a depth of 10~15 m below the surface) until 2/3 Q_n. As the applied load increased to net failure load (Q_n), the skin friction was also increased throughout the whole shaft depth and the maximum unit friction was mobilized at the depth of 9 ~ 10 m below the surface near the boundary of the two rock layers.

5. Conclusions

A series of centrifuge model test was performed to investigate the uplift response of the drilled shaft socketed in various strength of rocks. Experimental measurements were enabled to study the uplift load-displacement response, axial load distributions in the shaft, and unit skin friction distributions and the following conclusions were drawn:

• The uplift capacity of drilled shaft increased with an increase in the strength of rock-sockets. Stronger rock-socket resulted in resisting a greater load at a given displacement.

• The axial load in the shaft decreased slightly in the overlying sand layer and decreased steeply when the drilled shaft entered the underlying rock layer. Most of the applied load was carried in the underlying rock layer. When the drilled shaft is completely socketed in layered rock, both overlying layer and underlying layer shared applied load.

• Maximum unit friction was mobilized at a mid-depth of the underlying rock layer of the rock overlying sand layer.

• For layered rock sockets, the maximum unit friction was mobilized at the stronger underlying rock layer and then the skin friction increased along the shaft length with loading level.

Acknowledgments

This study was supported by the Korea Electric Power Research Institute under the R&D Program, project "Development of Reliability-Based Load and Resistance Factor Design (LRFD) Methods for foundations of transmission towers". This study was also partially supported by 2020 Research Grant from Kangwon National University.

References

AASHTO (2007), LRFD Bridge Design Specifications, American Association of State Highway and Transportation Officials.

Ashour, M. and Abbas, A. (2020), "Response of piles in multilayers of soil under uplift forces", *Int. J. Geomech.*, **20**(6), 04020056. https://doi.org/10.1061/(ASCE)GM.1943-5622.0001676.

ASTM (2006), D4254-00: Standard test method for minimum index density and unit weight of soils and calculation of relative density, ASTM International, West Conshohoken, Pennsylvania, U.S.A.

ASTM (2007), D3689-07: Standard Test Methods for Deep Foundations Under Static Axial Tensile Load, ASTM International; West Conshohoken, Pennsylvania, U.S.A.

ASTM (2007), D1557 07: Standard Test Methods for Laboratory Compaction Characteristics of Soil Using Modified Effort, ASTM International, West Conshohoken, Pennsylvania, U.S.A.

ASTM (2014), D4254-14: Standard Test Methods for Maximum Index Density and Unit Weight of Soils Using a Vibratory Table, STM International; West Conshohoken, Pennsylvania, U.S.A.

Carter, J.P. and Kulhawy, H. (1988), "Analysis and design of drilled shaft foundations socketed into rock", No. EPRI-EL-5918, Electric Power Research Inst., Palo Alto, California, U.S.A., Cornell University, Ithaca, New York, U.S.A.

Chang, C., Zoback, M.D. and Khaksar, A. (2006), "Empirical relations between rock strength and physical properties in sedimentary rocks", *J. Petrol. Sci. Eng.*, **51**(3-4), 223-237. https://doi.org/10.1016/j.petrol.2006.01.003.

Chellis, R.D. (1961), *Pile Foundations*, McGraw-Hill, New York, U.S.A.

Dykeman, P. and Valsangkar, A. (1996), "Model studies of socketed caissons in soft rock", *Can. Geotech. J.*, **33**(5), 747-759. https://doi.org/10.1139/t96-100-321.

El Naggar, M.H. and Wei, J.Q. (2000), "Uplift behaviour of tapered piles established from model tests", *Can. Geotech. J.*, **37**(1), 56-74. https://doi.org/10.1139/t99-090.

FHWA (2007), LRFD Bridge Design Specifications, FHWA-NHI-15-047, Federal Highway Administration.

Fuller F.M. (1983), *Engineering of Pile Installations*, McGraw-Hill, New York, U.S.A.

Gaaver, K.E. (2013), "Uplift capacity of single piles and pile groups embedded in cohesionless soil", *Alexandria Eng. J.*, **52**(3), 365-372. https://doi.org/10.1016/j.aej.2013.01.003.

Gao, F., Yan, W. and Ge, F. (2010), "Geotechnical investigation and tension-pile solution for foundation of SFT prototype at Qiandao Lake", *Procedia Eng.*, **4**, 127-134. https://doi.org/10.1016/j.proeng.2010.08.015.

Goel, S. and Patra, N.R. (2007), "Prediction of load displacement response of single piles under uplift load", *Geotech. Geol. Eng.*, **25**(1), 57-64. https://doi.org/10.1007/s10706-006-0006-3.

Hirany, A. and Kulhawy, F.H. (1988), "Conduct and interpretation of load tests on drilled shaft foundations: Volume 1, Detailed guidelines", Report EL-5915-V1, Electric Power Research Institute.

Horvath, R.G. and Kenney, T.C. (1979), "Shaft resistance of rock-socketed drilled piers", *Proceedings of the Symposium on Deep Foundations*, Atlanta, Georgia, U.S.A., October.

IEEE (2001), Std 691-2001: IEEE guide for transmission structure foundation design and testing, The Institute of Electrical and Electronics Engineers, New York, U.S.A.

Kim, D.S., Kim, N.R., Choo, Y.W. and Cho, G.C. (2013), "A newly developed state-of-the-art geotechnical centrifuge in Korea", *KSCE J. Civ. Eng.*, **17**(1), 77-84. https://doi.org/10.1007/s12205-013-1350-5.

Kim, J.H., Choo, Y.W., Kim, D.J. and Kim, D.S. (2016), "Miniature cone tip resistance on sand in a centrifuge", *J. Geotech. Geoenviron. Eng.*, **142**(3), 04015090. https://doi.org/10.1061/(ASCE)GT.1943-5606.0001425.

Kim, Y. and Rosher, L.T. (2019), "Performance of novel dynamic installed anchors during installation and monotonic pullout", *Geomech. Eng.*, **18**(2), 153-159. http://doi.org/10.12989/gae.2019.18.2.153.

Kishida, H. and Uesugi, M. (1987), "Tests of the interface between sand and steel in the simple shear apparatus", *Géotechnique*, **37**(1), 45-52. https://doi.org/10.1680/geot.1987.37.1.45.

Korea Institute of Civil Engineering and Building Technology (KICT) (2017), *2017 Standard Estimation System*, Ministry of Land, Infrastructure and Transport, Sejong City, South Korea.

Kulhawy, F.H. and Carter, J.P. (1992), *Socketed Foundations in Rock Masses*, in *Engineering in Rock Masses*, Butterworth-Heinemann, Oxford, U.K.

Kulhawy, F.H. (1991), *Drilled Shaft Foundations in Foundation Engineering Handbook*, Springer, Boston, Massachusetts, U.S.A.

Kulhawy, F.H. (2004), "On the axial behavior of drilled foundations", *Proceedings of the GeoSupport Conference 2004*, Orlando, Florida, U.S.A., January.

Lee, M.H., Cho, C.H., Yoo, H.K. and Kwon, H.K. (2003), "A study on the surface roughness of drilled shaft into rock in Korea", *Proceedings of the Korean Geotechnical Society Conference*, Seoul, South Korea, January.

Leung, C.F. and Ko, H.Y. (1993), "Centrifuge model study of piles socketed in soft rock", *Soils Found.*, **33**(3), 80-91. https://doi.org/10.3208/sandf1972.33.3_80.

Livneh, B. and El Naggar, M.H. (2008), "Axial testing and numerical modeling of square shaft helical piles under compressive and tensile loading", *Can. Geotech. J.*, **45**(8), 1142-1155. https://doi.org/10.1139/T08-044.

Park, S. (2018), "Evaluation of uplift behavior for drilled shaft socketed into rock via centrifuge model tests", Master Thesis, Korea Advanced Institute of Science and Technology, Daejeon, Korea

Prakash, S. and Sharma, H.D. (1990), *Pile Foundations in Engineering Practice*, John Wiley & Sons, Hoboken, New Jersey, U.S.A.

Pu, S., Zhu, Z. and Wei, W. (2020), "A method for calculating the ultimate bearing capacity of uplift piles in combined soil and rock mass", *Eur. J. Environ. Civ. Eng.*, 1-26. https://doi.org/10.1080/19648189.2020.1754296.

Reese, L. and O'Neill, M. (1988), "Drilled shafts: Construction and design", FHWA-SA-HI-88-042, Federal Highway Administration.

Rosenberg, P. and Journeaux, N.L. (1976), "Friction and end bearing tests on bedrock for high capacity socket design", *Can. Geotech. J.*, **13**(3), 324-333. https://doi.org/10.1139/t76-033.

Rowe, R.K. and Armitage, H.H. (1987), "A design method for drilled piers in soft rock", *Can. Geotech. J.*, **24**(1), 126-142. https://doi.org/10.1139/t87-011.

Tomlinson, M.J. (1977), *Pile Design and Construction Practice*, Cement and Concrete Association, U.K.

Yang, B., Ma, J., Chen, W. and Yang, Y. (2018), "Uplift behavior of belled short piles in weathered sandstone", *Math. Prob. Eng.*, 8614172. https://doi.org/10.1155/2018/8614172.

Yarramsetty, P.C.R., Domala, V., Poluraju, P. and Sharma, R. (2019), "A study on response analysis of submerged floating tunnel with linear and nonlinear cables", *Ocean Syst. Eng.*, **9**(3), 219-240. https://doi.org/10.12989/ose.2019.9.3.219.

Xing, H., Zhang, Z., Meng, M., Luo, Y. and Ye, G. (2014), "Centrifuge tests of superlarge-diameter rock-socketed piles and their bearing characteristics", *J. Bridge Eng.*, **19**(6), 213-226. https://doi.org/10.1061/(ASCE)BE.1943-5592.0000582.